

## Shape memory alloy-based small crawling robots inspired by *C. elegans*

This article has been downloaded from IOPscience. Please scroll down to see the full text article.

2011 Bioinspir. Biomim. 6 046002

(<http://iopscience.iop.org/1748-3190/6/4/046002>)

View [the table of contents for this issue](#), or go to the [journal homepage](#) for more

Download details:

IP Address: 143.248.135.34

The article was downloaded on 13/10/2011 at 02:18

Please note that [terms and conditions apply](#).

# Shape memory alloy-based small crawling robots inspired by *C. elegans*

Hyunwoo Yuk<sup>1</sup>, Daeyeon Kim<sup>1</sup>, Honggu Lee<sup>2</sup>, Sungho Jo<sup>2</sup> and Jennifer H Shin<sup>1</sup>

<sup>1</sup> Department of Mechanical Engineering, Korea Advanced Institute of Science and Technology, 291 Daehak-ro, Yuseong-gu, Daejeon, Korea,

<sup>2</sup> Department of Computer Science, Korea Advanced Institute of Science and Technology, 291 Daehak-ro, Yuseong-gu, Daejeon, Korea

E-mail: [shjo@kaist.ac.kr](mailto:shjo@kaist.ac.kr) and [j\\_shin@kaist.ac.kr](mailto:j_shin@kaist.ac.kr)

Received 23 May 2011

Accepted for publication 30 August 2011

Published 12 October 2011

Online at [stacks.iop.org/BB/6/046002](http://stacks.iop.org/BB/6/046002)

## Abstract

Inspired by its simple musculature, actuation and motion mechanisms, we have developed a small crawling robot that closely mimics the model organism of our choice: *Caenorhabditis elegans*. A thermal shape memory alloy (SMA) was selected as an actuator due to the similarities of its properties to *C. elegans* muscles. Based on the anatomy of *C. elegans*, a 12-unit robot was designed to generate a sinusoidal undulating motion. Each body unit consisting of a pair of SMA actuators is serially connected by rigid links with an embedded motion control circuit. A simple binary operation-based motion control mechanism was implemented using a microcontroller. The assembled robot can execute *C. elegans*-like motion with a 0.17 Hz undulation frequency. Its motion is comparable to that of a real worm.

(Some figures in this article are in colour only in the electronic version)

## 1. Introduction

Biologically inspired robots have been attracting a growing number of robotics researchers for the last few decades. Themes in the study of biomimetic robotics borrow design concepts of structures, sensors and actuators from animals. In the field of intelligent robotics, many attempts have been made to mimic the actuation mechanism of snakes [1], lampreys [2] and salamanders [3]. For example, many investigators have developed robotic snakes of various sizes and functions to emulate their simple undulating motion. However, the musculature and corresponding motion mechanisms of a snake are very complex and technically challenging to mimic in robotic applications. Therefore, most snake-like robot designs rely largely on traditional electrical motor-based actuation mechanisms, which involve complexity in implementation and are often remote from that living organism's muscle-based system [4, 5]. Because most animals utilize a number of small muscle cells that coordinate their work to generate motion, a series of micro-linear actuators would represent its motion better than an electrical motor. The electrical motor-based actuation also imposes constraints on the size and weight of

the robots, especially in trying to miniaturize them. Therefore, recent efforts have been made by a number of investigators to design actuators that are not only functionally comparable to living organisms but also structurally and materially versatile in overcoming these constraints. As a result, smart materials such as shape memory alloys (SMAs) [6–10], electro-active polymers [11] and ionic polymer metal composites (IPMCs) [12] have been employed as promising candidate substances for actuators to engender natural motions of biologically inspired small-sized robots.

As a model organism for a crawling robot, we have chosen *Caenorhabditis elegans*, which is a 1 mm long soil nematode whose body consists of several hundreds of cells without any rigid skeletal structures. *C. elegans* is a good model organism because of its biologically simple structure and because the characteristics of its motion are well investigated [13]. The motion of *C. elegans* is executed by contraction and relaxation of its internal body wall muscles. As shown in figure 1(a), the cross-sectional image of the worm features four quadrants of muscle rows along its body: two rows on the dorsal side and two on the ventral side. By dorso-ventral

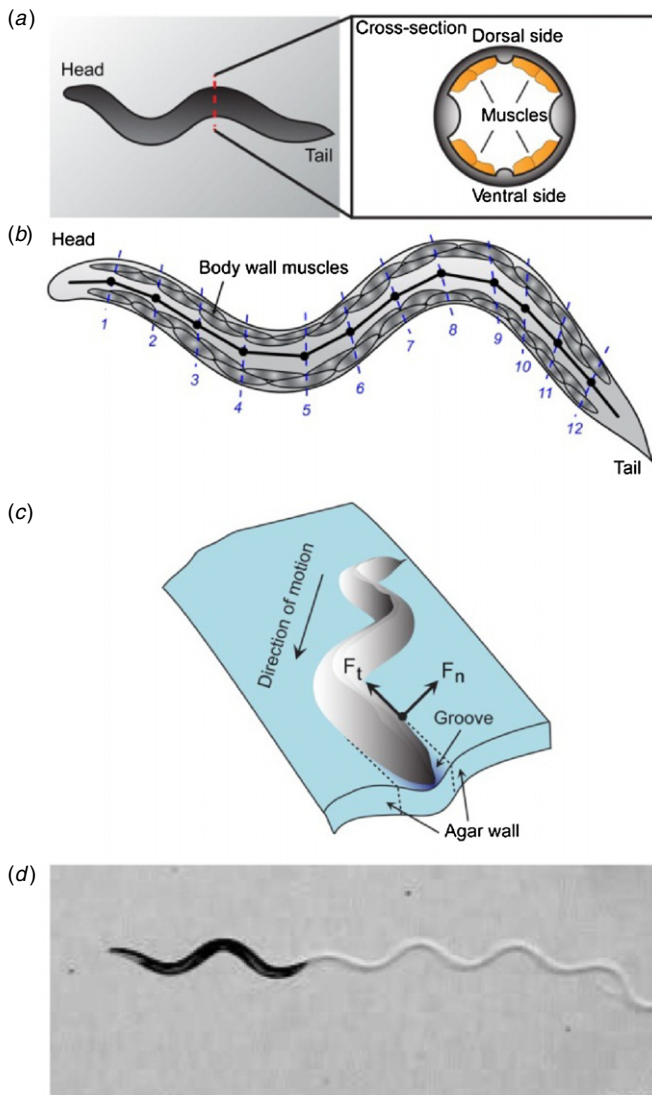


**Figure 1.** (a) A cross-sectional image of the worm shows that the muscle cells form four quadrants of muscle rows along its body: two rows on the dorsal side and two on the ventral side. (b) Longitudinally, an array of 24 overlapping muscle cell units runs on each of the dorsal and ventral sides of the worm. (c) Higher normal friction ( $F_n$ ) than tangential friction ( $F_t$ ) causes frictional anisotropy. (d) A crawling *C. elegans* on an agar plate exhibits locomotion with a simple sinusoidal body wave and very smooth movement without much lateral slipping.

flexing of these wall muscles, the worms generate sinusoidal body waves [14]. Longitudinally, an array of 24 overlapping muscle cell units runs on each of the dorsal and ventral sides of the worm (figure 1(b)). During worm locomotion, a sinusoidal body wave propagates along the worm's body in the opposite direction from its movement similar to a snake or an eel, and its undulation characteristics such as wavelength, amplitude, frequency and velocity are heavily affected by environmental parameters as it moves [15]. For example, when their amplitude is limited by regularly spaced obstacles or a narrow channel similar to their natural environment in humid soil, the worm's velocity can be greatly enhanced [16, 17]. Also, when the worm crawls on an agar plate in

a laboratory setting, the worm's body presses against the agar surface to form an impression due to the surface tension of the water film. The walls of the agar groove can generate a frictional anisotropy whose normal friction is much higher than its tangential friction (figure 1(c)). In this condition, the worm exhibits locomotion with a simple sinusoidal body wave and very smooth movement without much lateral slippage at its locomotion frequency of approximately 0.5 Hz as shown in figure 1(d) [18]. However, when the worm is placed on a rigid surface with a relatively shallow impression featuring reduced frictional anisotropy, it cannot propel itself forward appreciably using a sinusoidal body wave [14]. That is, *C. elegans* can generate a simple sinusoidal body wave on a plane using its dorso-ventral musculature, but its movement is determined by external environmental conditions.

Inspired by its simple musculature, actuation and locomotion mechanisms, we developed a small crawling robot that closely mimics the model organism of our choice: *C. elegans*. Not only can we mimic the muscle's arrangement and motion mechanisms with a simple control scheme, but the simplicity of the worm's structure and motion is also beneficial in reducing the size of the crawling robot compared to motor-based snake robots. In this paper, we aim to introduce a bio-mimetic robot design inspired by a crawling nematode *C. elegans* with four objectives: (1) to design a small-sized and low-weight crawling robot, (2) to mimic the actual muscles and their motion, (3) to create a motion generation algorithm that can easily be implemented using simple hardware and (4) to understand the dynamic characteristics of the model organism through hardware manufacturing. In our preliminary study [7], we built a four-segmented prototype robot to test the feasibility of our approach. This paper presents a much more advanced full-bodied robot by improving the body material and processing technique, which utilizes 3D rapid prototyping and the code for motion generation. In addition, experiments to evaluate the motion characteristics of the robot were conducted.

## 2. Actuator material selection

Each row of the body wall muscles of *C. elegans* consists of interconnected muscle cells. The worm's sinusoidal flexure is the consequence of the cooperative contraction and relaxation of several muscle cells lining the dorsal and ventral sides of the body, which generate a maximum contraction of approximately 50% [19]. Therefore, each muscle cell of the worm can be considered as a flexible linear actuator that is connected to the neural system, while the entire worm can be regarded as a multi-DOF system consisting of several elastic linear actuators. To mimic the worm's musculature and its motion, small-sized flexible linear actuators would be desirable.

Many biologically inspired robots utilize electric motors for actuation. Linear electric motors can generate a highly robust linear movement, but this movement usually consists of rigid components, and there is difficulty using these motors in the length scales of several centimeters. Although rotational electric motors are most commonly used for robotic

**Table 1.** List of available smart materials and their potential problems [20–24].

Materials	Potential problems
Dielectric elastomers	Require high voltage (>1 kV)
Relaxor ferroelectric polymers	Require high voltage (>1 kV)
Liquid crystal elastomers	Slow response, high field requirement (1–25 MV m <sup>-1</sup> )
Conducting polymers	Require encapsulation
Molecular actuators	Slow response, need encapsulation
Carbon nanotubes	Small strain (0.2% typ.), expensive material
IPMCs	Require encapsulation, small force generation
Piezoelectric actuators	Poor strain
Ferromagnetic SMAs	Require bulky magnets

applications due to their high functionality and robustness, their mechanism is still far from an actual worm's muscle-based actuation.

Therefore, a number of different smart materials have been considered for a flexible linear actuator instead of bulky and rigid electric motors. Recent studies have shown that robots with smart material-based soft actuators can be both functionally versatile and structurally comparable to model organisms such as earthworms or lampreys [2, 6]. To select an appropriate smart material for our purpose, several functional requirements and practical issues are considered. From a functional point of view, a worm's body wall muscles should be able to generate at most a 50% contraction of its original length like the actual worms [19]. From a practical point of view, low-voltage actuation at a low cost with commercially available products would be preferred. Table 1 shows a list of commonly used smart materials and the potential problems in implementation for small robot development. Each smart material in the list has its own advantages, but they are inappropriate for our purpose because of the listed potential problems. For instance, a dielectric elastomer, despite its advantageous properties such as large strain, low cost, low current and a high electro-mechanical efficiency, has a major weakness for our purpose due to its high voltage requirement (over 1 kV dc–dc) because utilizing multiple actuators with very high dc–dc voltage requirements would not be practical [20, 23]. Conducting polymers, however, are not suitable for a small-sized actuator due to their encapsulation requirement and small strain (<2%) despite their several promising advantages. While IPMCs are an emerging soft material for many biologically inspired robots such as worm-like robots [12], the bending actuation of an IPMC is not appropriate for a contraction–relaxation-based linear actuator. Also, IPMCs have an encapsulation problem as well as disadvantages from a practical standpoint, specifically in their high cost and complicated fabrication process.

For our design, thermally actuated SMAs are selected as an actuation material. In a linear configuration, its deformation is as little as 5% of its original length; but in a coiled spring-like configuration, its deformation can be increased up to 50% of its original length, which is approximate to

the muscle property of the worm. Typical thermal SMAs can be stretched by applying an external force and return to their original configuration elastically when their temperature is increased above a threshold; thus, they exhibit a binary operating property. Because *C. elegans* muscles produce a constant force regardless of their length and generate simple undulations by contraction and relaxation [19], the binary operation property of a thermal SMA is comparable to the worm's muscular operation. Moreover, according to the reported computational motion simulation of *C. elegans* [5], the sequential operation of serial binary positioning actuators is suitable to generate the sinusoidal motion of the worm. From a practical standpoint, thermal SMAs are commercially accessible at a relatively low cost compared to other smart materials and their contraction force is large enough for small-sized applications. Based on these considerations, a thermal SMA was selected as a promising linear actuator for the development of a small crawling robot inspired by *C. elegans*.

### 3. Design and assembly

As shown in figure 1(b), *C. elegans* has 24 body wall muscle cells in a row on the dorsal or ventral sides. Therefore, Wakabayashi's computational simulation of *C. elegans* motion uses a model consisting of 24 segments of spring-damper units [19]. Although actual *C. elegans* has 24 body wall muscle cells in each row, half of them are overlapped with each other, which allows other researchers to model the body with 12 body segments [25]. Based on the dynamic model proposed by Suzuki [25], we designed a robot with 12 body segments. The bending motion of each body segment is generated by a pair of dual spring units in which each of the spring units mimics the dorsal and the ventral side of the body wall muscle. The robot design is explained in three steps: (1) thermal SMA-based linear actuator design, (2) robot body unit design and (3) integrated robot structural design.

#### 3.1. Design of a thermal SMA-based linear actuator

In this study, we utilized a commercially available thermal SMA: Biometal® Helix (BMX150) manufactured by Mondo-Tronics, Inc. We first decided on the size of the robot based on manufacturability and suitability of assembly. Given the availability of the SMA spring suitable for emulation of contractile muscles, we chose our SMAs to be able to generate enough force for the prescribed size. The fully contracted length of the SMA spring is 5 mm, the outer diameter of the helix is 0.62 mm, the wire diameter is 150 μm and the activation temperature is 70 °C. At room temperature, the SMA spring can be elongated to approximately 1 cm. When a current is fed through it, it can contract up to 50% of its extended length, producing a maximum force of approximately 0.3 N. Because this SMA features an irreversible process and requires an external force to recover its deformation to the relaxed state, we combined it with a passive spring, whose original length is twice that of the fully contracted SMA spring, in a parallel configuration to the thermal SMA spring to create a single linear actuator unit (figure 2(a)). The operation of the SMA-based linear actuator can be divided into an activation stage

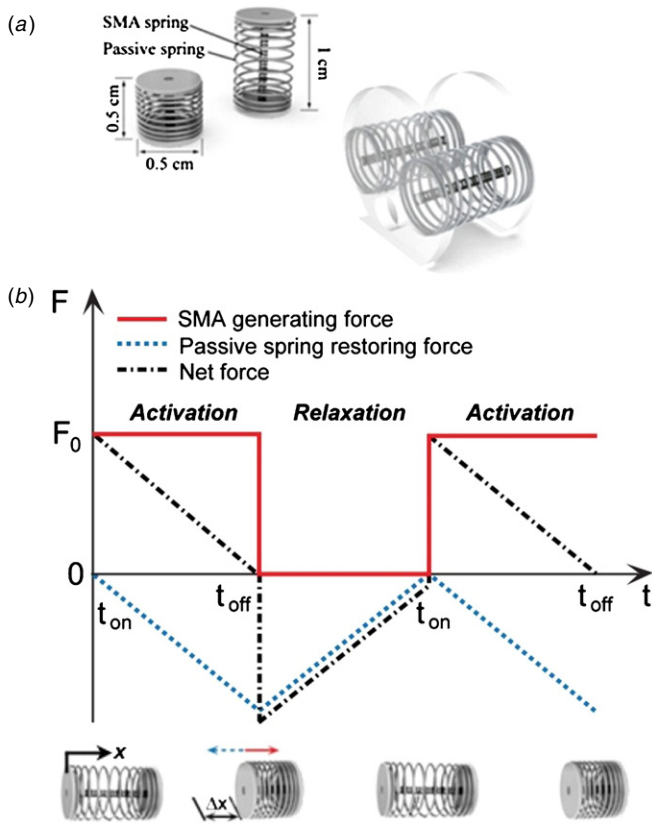


**Figure 2.** (a) The actuator unit is made from a pair of dual springs (a SMA spring and a passive bias spring): the blown-up images show the contracted (left) and the relaxed (right) states of a single linear actuator unit. (b) Schematic representation of the force generated by the SMA spring (solid line),  $F_0$ , restoration force by a passive spring (dotted line) and the net force (dash-dotted line) during the contraction (current supply on) and relaxation (current supply off) states. Given the spring constant of our passive spring ( $k = 60 \text{ N m}^{-1}$ ) and the maximum deformation (0.5 cm), the maximum restorative force for the passive spring can be calculated.

and a relaxation stage. During the activation stage, an electric current is supplied to the SMA spring and its temperature is elevated by the current passing through the SMA. Then, it contracts when the temperature of SMA exceeds its threshold temperature. During the relaxation stage, the current through the SMA is blocked, and the SMA is restored to its stretched length by the passive spring while it is cooling down. During the contraction, if the supplied electric current is too low, it will take too long to reach the threshold temperature, resulting in an additional delay before contraction. If the supplied current is too high, the SMA spring will overheat. The appropriate current of 200 mA was empirically chosen to achieve a balance between activation and relaxation time and to avoid overheating during operation.

Figure 2(b) shows a schematic representation of the force generated by the SMA spring (solid line), the restoration force by the passive spring (dotted line) and the net force (dash-dotted line) during the contraction (current supply on) and relaxation (current supply off) states. Because the SMA spring can generate a maximum force of 0.3 N and its contracted length is 0.5 cm, we selected a passive spring whose spring coefficient is  $60 \text{ N m}^{-1}$ . At the maximally contracted state,

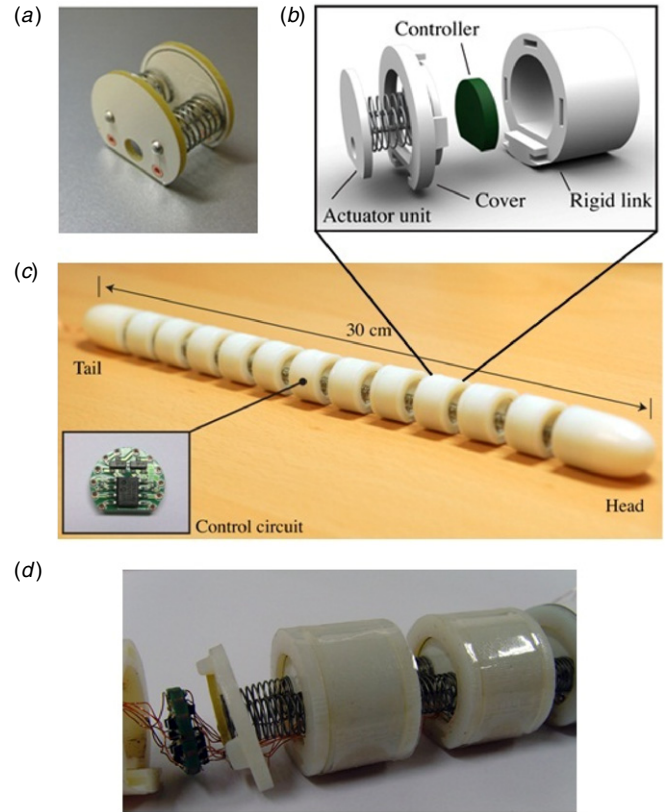


**Figure 3.** The assembly of the crawling robot: (a) each actuator is fabricated using a PCB, and a dual spring unit consisting of the SMA spring, and a passive spring is soldered to the PCB part. (b) Each segment of the robot consists of an actuator unit and a controller encapsulated by a cover and a hollow rigid link. (c) Assembled crawling robot consisting of 12 body segments. (d) Wired circuitry and actuator unit.

zero residual force, i.e. the net force between the contraction force of the SMA spring and the elastic force of the passive bias spring, is retained to provide enough force during robot locomotion.

### 3.2. Robot body unit fabrication and assembly

Each actuator is fabricated using a printed circuit board (PCB) and a dual spring unit consisting of the SMA spring and a passive spring soldered to the PCB part, as shown in figures 3(a) and (b). PCB fabrication enables convenient assembly and provides robustness to the heat from the SMA. The linear actuation units are then serially connected to each other with a rigid link between in order to form the *C. elegans* robot (figure 3). The rigid link is designed as a circular cylindrical shape with a flattened bottom for stability of the robot on the ground. The link is hollow to allow wires to pass through as shown in figure 3(a). The actuator control circuitry is placed inside the hollow casing that acts as a rigid link. The actuator unit is fixed to the rigid link by two covering pieces. All the body parts are fabricated by rapid prototyping using acrylonitrile-butadienestyrene (ABS) plastic for its manufacturability of 3D objects as well as its good resistance to heat.

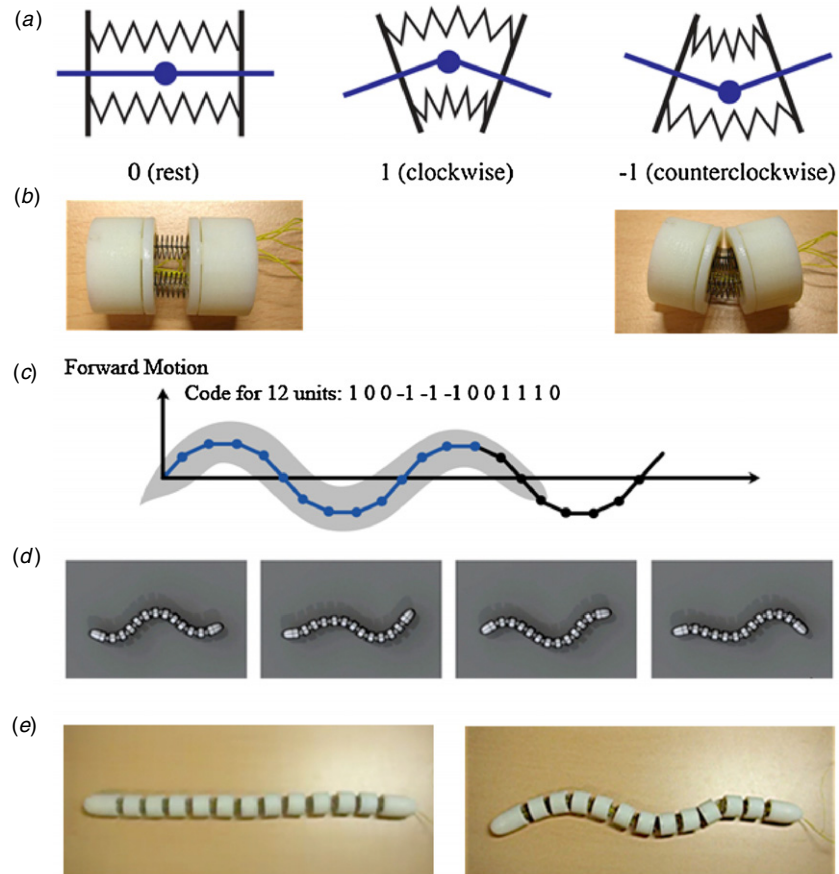


**Figure 4.** (a) The schematic of the three motion modes of a single actuator unit. (b) Images of the motion modes of the real actuator unit for resting and counterclockwise bending stages. (c) An example of the sequential motion code for forward motion. (d) A sequence of frames illustrating the computational simulation result of forward motion control captured every 4 s. (e) Images of the motion modes of the robot with 12 body segments.

### 3.3. Whole robot integration

Suzuki [25] proposed a *C. elegans*' dynamic simulation model with 12 segments. Twelve body segments are adequate to mimic a longitudinal array of 24 overlapping muscle cell units. Therefore, our robot was designed with 12 rigidly linked segments, each of which consists of two dual spring units and a microcontroller whose dimensions are 1.4 cm × 1.2 cm (width × height). The resulting 12-segmented robot has a size of 30 cm × 2 cm × 1.5 cm (length × width × height) and has a weight of 50 g (figure 3(c)).

The actuator control circuitry is connected through insulated fine copper wires ( $\phi 0.16$  mm) for power supply and to receive electric input commands (figure 3(d)). Two wires from each controller are soldered to the SMA spring. A microcontroller in a rigid body link delivers the input command to the microcontroller in the adjacent body link through copper wires. The sequential signal delivery is explained in detail in section 4.2. In total, three wires (microcontroller power supply, actuator power supply and ground) are embedded into the tail part of our robot to transfer input commands. To drive the desired current of 200 mA, the controller and actuator are powered separately at 5 and 3 V, respectively.

## 4. Motion control method

### 4.1. Motion control mechanism

Because our robot utilizes thermal SMA springs, the operation of each actuator unit has a binary operational property. Limited by the size of the robot, a complex feedback control method, which would require excessive computing power, would be inappropriate for the motion control. Although the pulse width modulation method is widely used for thermal SMA applications to prevent overheating of the SMA, this again has difficulties in implementation in small-sized hardware [26]. Instead of complex control methods, we propose a simple sequential binary positioning mechanism to generate a sinusoidal waveform. A specific sequence of codes corresponds to a specific motion mode, and a repeating cycle of this sequence can produce sinusoidal undulation of the robot.

Each body segment is regarded as a rotating joint. A SMA spring in the actuator unit is activated individually to generate a certain angle of flexure: either clockwise or counterclockwise. We can assign numeric codes (0, 1 and -1) in order to distinguish the three different configurations as illustrated in figure 4(a), where 0, 1 and -1 represent resting, clockwise bending and counterclockwise bending, respectively. With two parallel dual spring units, the bending

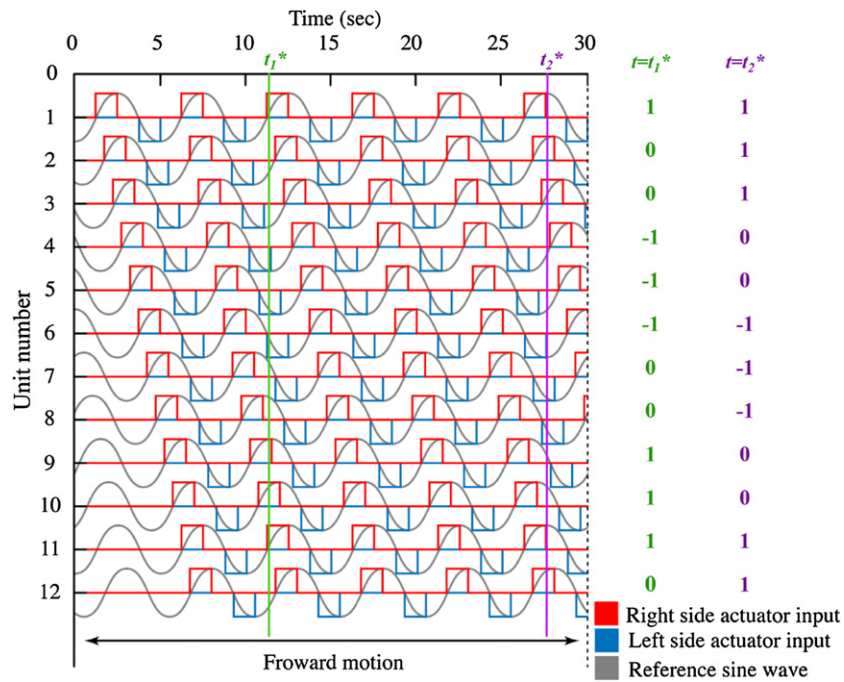


**Figure 5.** Code sequence of the 12 actuator units as a function of time: all of the 12 actuator units receive repeating code sequence of 1, 0, -1, 0, . . . with a delay of 0.6 s between two consecutive signals. At a given moment in time, for instance at  $t = t_1^*$ , the code sequence over the 12 body units becomes 1, 0, 0, -1, -1, -1, 0, 0, 1, 1, 1, 0 as shown in figure 4(c), resulting in a sinusoidal wave. Similarly, at  $t = t_2^*$ , the code sequence will be 1, 1, 1, 0, 0, -1, -1, -1, 0, 0, 1, 1.

motion implementation is tested by activating one of the two dual spring units as shown in figure 4(b). We can produce the desired motion by assigning the proper code sequence. The forward motion sequence shown in figure 4(c) generates a sinusoidal wave whose computational simulation using Solidworks Motion (Solidworks Corp.) and experimental results are shown in figures 4(d) and (e), respectively

4.2. Control method implementation

The proposed motion control method is simple enough to be operated with simple circuitry using a microcontroller (PIC12F629 from Microchip, Inc.). The implemented controller is an open-loop controller without any feedback signal and employs a constant current circuit because activation of SMAs is sensitive to current flow and its resistance changes during operation as shown in the inset in figure 3(c). The controller can produce a step electric input command of approximately 200 mA in amplitude and 1.5 s in duration. The operating current input is represented by a numeric code. The control algorithm is programmed to generate the abovementioned code sequences. To execute forward movement, for example, the first actuator unit receives a repeating code sequence of 1, 0, -1 0, . . . and the second body unit receives the identical code sequence to the first unit with a delay of 0.6 s. This time-shift is empirically selected to successfully generate the sine-wave motion. Our proposed sequence code generates the robot’s sine-wave motion, and the 0.6 s shift implements the sequence code in reality. Consequentially, a subsequent actuator unit receives the same code sequence as that of the previous actuator unit with a

delay of 0.6 s. Figure 5 illustrates the code sequence of 12 actuator units as a function of time. At a given moment in time, for instance at  $t = t_1^*$ , the code sequence over the 12 body units becomes 1, 0, 0, -1, -1, -1, 0, 0, 1, 1, 1, 0 as shown in figure 4(c), resulting in a sinusoidal wave. Similarly, at  $t = t_2^*$ , the code sequence will be 1, 1, 1, 0, 0, -1, -1, -1, 0, 0, 1, 1. In other words, at any moment in time, 12 units will show any sequence in the repeating sequence of (1, 1, 1, 0, 0, -1, -1, -1, 0, 0, 0)<sub>n</sub>. The generated sinusoidal wave’s length and amplitude are 25 and 3 cm respectively. As shown in figure 5, the period of the sinusoidal wave is 6 s, which is equivalent to a frequency of approximately 0.17 Hz, which is within the same order of magnitude as an actual worm undulation. In addition to a simple running motion, a turning motion of the robot can be achieved by modifying the code sequence to locally change the period of the sinusoidal wave.

5. Experimental results

When the robot moves on an unbounded 2D planar surface, it is unable to push its body forward appreciably due to lateral slippage similar to the actual worms moving on a rigid surface lacking frictional anisotropy. By constructing walls whose width is smaller than the typical amplitude of the robot undulation, we can reinforce the tangential and normal forces at the contact to obtain forward directional thrust and confine its movement in a steady manner (figures 6(a) and (b)). The channel width is selected to be 2.5 cm empirically taking into account the sine-wave amplitude of 3 cm for the freely moving

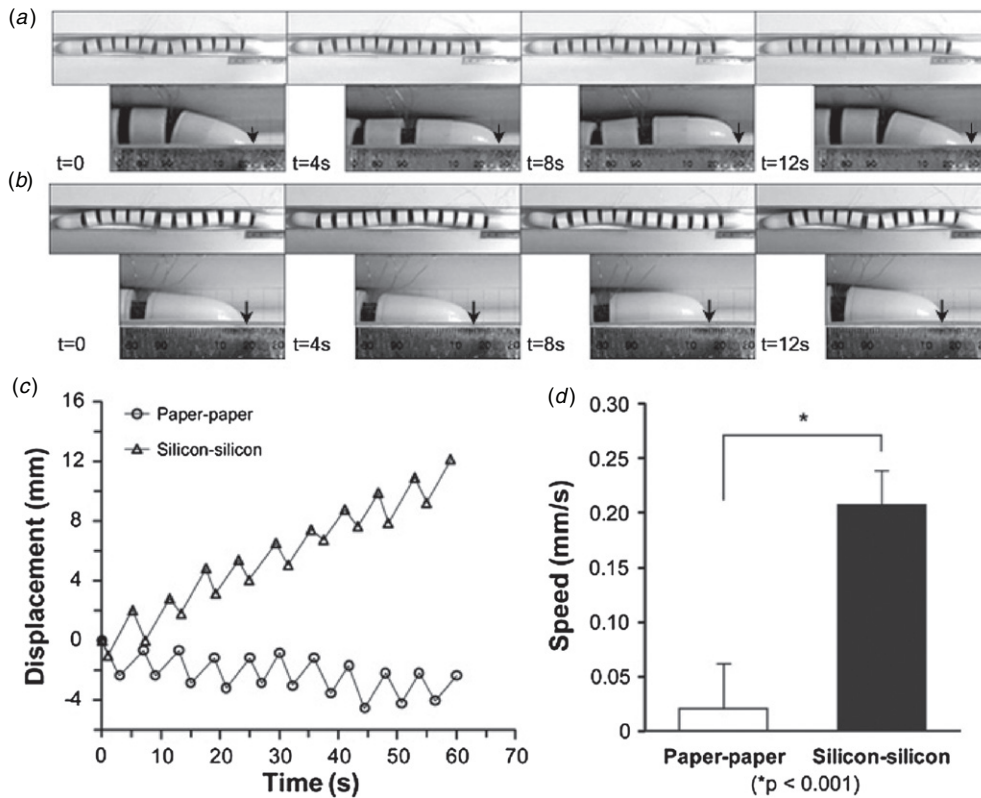


**Figure 6.** Sequential images of the crawling robot captured every 4 s in the channel with (a) silicone–silicone contacts and (b) paper–paper contacts. (c) A representative displacement profile of the robot in both silicon–silicon contact and paper–paper contact conditions. While the robot with large wall friction with the silicon–silicon contacts can move forward with oscillations due to contraction, the robot with small wall friction with the paper–paper contact condition does not seem to generate enough force to move forward. (d) The average speed of the robots ( $n = 5$  for each condition) measured over 60 s indicates significant difference depending on the environmental conditions.

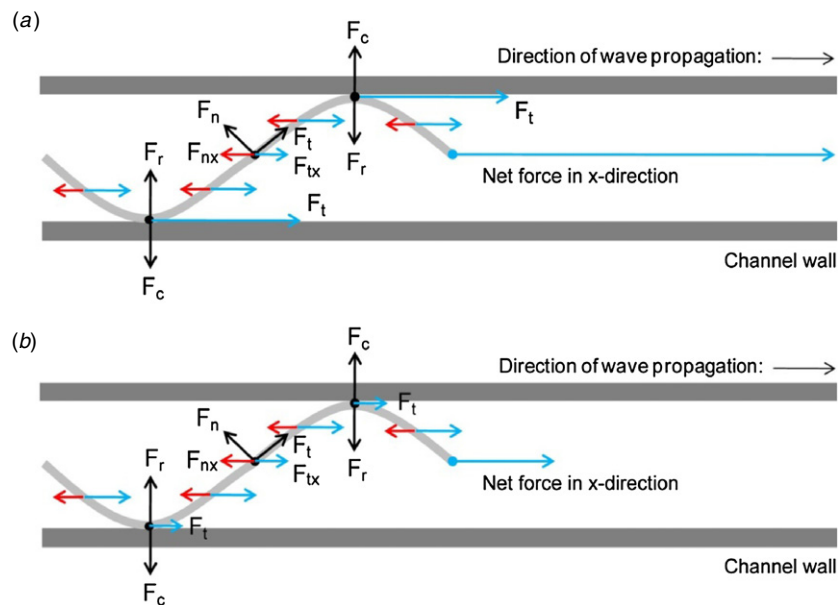


**Figure 7.** Free body diagrams for the crawling motions of the robots in the channel with different surfaces. The surfaces of the robot body and channel wall are silicone (a) and paper (b). The surfaces of the bottoms in (a) and (b) are paper.  $F_c$  is the contact force at the contact point between the wall and robot body.  $F_r$  is the reaction force to  $F_c$ .  $F_n$  and  $F_t$  are the normal and tangential friction forces, respectively. The red and blue arrows indicate the projections to the  $x$ -axis of  $F_n$  and  $F_t$ , respectively.

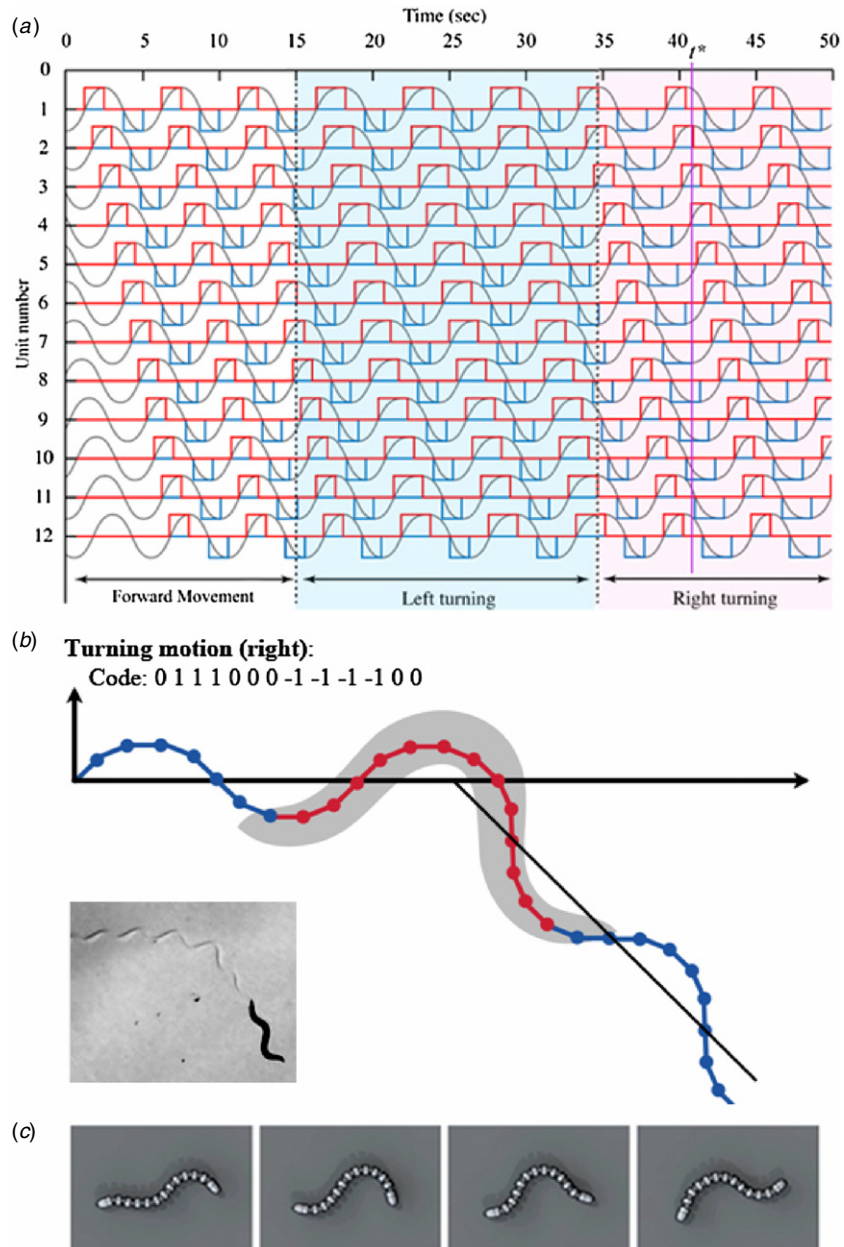


**Figure A1.** (a) Code sequence of the 12 actuator units as a function of time to generate forward and turning motions. (b) The sequential motion codes for turning motion. The inset shows a real image of a turning *C. elegans*. (c) A sequence of frames illustrating the computational simulation result of right turning motion control captured every 4 s.

robot. If the channel were either narrower or wider, the robot would not move fluidly.

To increase the tangential frictional force at the contact, both the channel wall and the robot were covered with a silicon sheet (Kuraray, Japan). The robot, enclosed by silicon, moved forward in the silicon walled channel with a saw-tooth-like pattern due to the contraction–relaxation pattern of body segments as shown in figures 6(a) and (c). The snapshots in figure 6(a) were taken every 4 s and the robot’s head location is indicated by an arrow to show the forward movement. To validate the effect of frictional force, which contributes to movement generation, the robot with a paper–paper contact condition is also tested. The snapshots demonstrate that the

robot made no significant forward movement on average. The comparison between these two different contact conditions in terms of displacement and speed is shown in figures 6(c) and (d). For the silicon–silicon contact condition, the robot moves at an average speed of  $0.21 \text{ mm s}^{-1}$ , while the paper–paper contact condition results in an average speed of  $0.02 \text{ mm s}^{-1}$ . Figure 7 illustrates the force diagram for these two conditions and shows that the difference in the tangential frictional force at the contact leads to difference in net  $x$ -directional force. The silicon–silicon contact condition generates a larger wall friction than the paper–paper contact condition and generates a forward net thrust force to move the robot forward. To verify the friction force difference between the two contact material

conditions, we measured the static frictional coefficients of two materials. An object of known mass was placed on a planar surface, which was then inclined until the object started moving. The tilt angle between the inclined plane and the ground was measured, and its tangent value was interpreted to be the frictional coefficient value. The contact between the plane surface and the mass was tested with the paper–paper and the silicon–silicon contact conditions. Through repeated experiments ( $n = 10$ ), we obtained the estimates of the static frictional coefficients. They were  $2.188 \pm 0.055$  and  $0.331 \pm 0.007$  for the silicon–silicon and paper–paper contacts, respectively. The estimated values are different by one order of magnitude, which gives rise to the differential frictional tangential force in these two conditions.

## 6. Conclusions

Our goal was to design a small-sized crawling robot that closely mimics the crawling motion of *C. elegans* and to generate response motions of the simple robot in an environment with different frictional conditions. The overall design of the robot includes two key features: (1) SMA-based actuation mimicking the body wall muscle anatomy of *C. elegans* and (2) a simple binary motion control mechanism inspired by the muscular activations of *C. elegans* during locomotion.

We first tested a four-segmented robot made of acrylic as the first prototype to check the feasibility of our design approach [7]. The current robot body was fabricated using a 3D rapid prototyping technique with ABS plastic, and the thermal SMA was soldered to a PCB to ensure a robust connection. The actuators were designed using a thermal SMA because it is reasonably comparable to the actual worm's wall muscles as well as its easy accessibility. The binary on-and-off activation of the SMA-based actuators mimicked the wall muscular activation. With the appropriate operation scheme coordination, the actuators successfully generated the desired body motions. With a simple control mechanism, the 12-segmented robot demonstrated *C. elegans*-like motions with a 0.17 Hz undulation frequency, which closely mimics the real worm. Similar to real worms, the movement of the robot was determined by the conditions of its environment. By constructing a wall with different frictional coefficients, we were able to make the robot move forward using its frictional anisotropy. Our results agree with the observation that actual crawling animals utilize natural obstacles such as soil particles to magnify the effect of anisotropic friction. In a previous study [10], the effects of friction in locomotion were investigated with a biomimetic robot inspired by the earthworm *Lumbricus terrestris*. While this robot moves using a peristaltic motion, our robot undulates by making a sinusoidal curve. Therefore, the contribution of frictional forces in executing forward motions is very different in these two cases.

## Acknowledgments

This work is supported in part by KAIST KI for Design of Complex Systems, Korean National Research Foundation

(NRF 2009-0073354, NRF 2010-0016886) and the Korean Government (MKE) under Human Resources Development Program for Convergence Robot Specialists.

## Appendix

In addition to a simple forward motion, the turning motion of the robot can be achieved by modifying the code sequence to locally change the period of the sinusoidal wave as illustrated in figure A1(a). During turning, the first actuator unit receives a code sequence 1, 0,  $-1$ , 0 repeatedly, which is similar to the forward motion. However, the code '1' lasts for 2.25 s instead of 1.5 s, while the duration for both '0' and ' $-1$ ' is still 1.5 s. The same code sequence is employed for the next actuator unit with a delay of 0.6 s. The extended duration of the right-side actuator results in a left turn, while the extended duration of the left-side actuator leads to a right turn, as shown in figure A1(b). We tested computational simulations to find an adequate code sequence to mimic a shallow turn of *C. elegans* (figures A1(b) and (c)) [27].

## References

- [1] Hirose S 1993 *Biologically Inspired Robots (Snake-like Locomotor and Manipulator)* (London: Oxford University Press)
- [2] Wilbur C, Vorus W, Cao Y and Currie S 2002 A lamprey-based undulatory vehicle *Neurotechnology for Biomimetic Robots* ed J Ayers, J Davis and A Rudolph (Cambridge, MA: MIT Press)
- [3] Ijspeert A J, Crespi A and Cabelguen J 2005 Simulation and robotics studies of salamander locomotion—applying neurobiological principles to the control of locomotion in robots *Neuroinformatics* **3** 171–95
- [4] Hirose S and Mori M 2004 Biologically inspired snake-like robots *Proc. IEEE Int. Conf. On Robotics and Biomimetics (Shenyang, China)* pp 1–7
- [5] Crespi A and Ijspeert A J 2008 Online optimization of swimming and crawling in an amphibious snake robot *IEEE Trans. Robot.* **24** 75–87
- [6] Menciassi A, Gorini S, Pernorio G and Dario P 2004 A SMA actuated artificial earthworm *ICRA 2004: Proc. 2004 IEEE Int. Conf. on Robots and Automation (New Orleans, USA)* pp 3282–7
- [7] Yuk H, Shin J H and Jo S 2010 Design and control of thermal SMA based small crawling robot mimicking *C. elegans* *Proc. IEEE/RSJ Int. Conf. on Intelligent Robots and Systems (Taipei, Taiwan, 18–22 October)*
- [8] Laschi C, Mazzolai B, Mattoli V, Cianchetti M and Dario P 2009 Design of a biomimetic robotic octopus arm *Bioinsp. Biomim.* **4** 015006
- [9] Trimmer B, Takesian A, Sweet B, Rogers C, Hake D and Rogers D 2006 Caterpillar locomotion: a new model for soft-bodied climbing and burrowing robots *Proc. Int. Symp. Technology and the Mine Problem (Monterey, CA, USA)*
- [10] Menciassi A, Accoto D, Gorini S and Dario P 2006 Development of a biomimetic miniature robotic crawler *Auton. Robot.* **21** 155–63
- [11] Bar-Cohen Y 2002 Electro-active polymers: current capabilities and challenges *Proc. SPIE NDE and Smart Structures Conf. (San Diego, USA)*
- [12] Arena P, Bonomo C, Fortuna L, Frasca M and Graziani S 2006 Design and control of an IPMC wormlike robot *IEEE Trans. Syst. Man Cybern. B* **36** 1044–52

- [13] Sauvage P, Argentina M, Drappier J, Senden T, Sime'on J and DiMeglio J-M 2010 An elasto-hydrodynamical model of friction for the locomotion of *Caenorhabditis elegans* *J. Biomech.* **44** 1117–22
- [14] White J G, Southgate E, Thomson J N and Brenner S 1986 The structure of the nervous system of nematode *Caenorhabditis elegans* *Phil. Trans. R. Soc. B* **314** 1–340
- [15] Berri S, Boyle J H, Tassieri M, Hope I A and Cohen N 2009 Forward locomotion of the nematode *C. elegans* is achieved through modulation of a single gait *HFSP J.* **3** 186–93
- [16] Lockery S R *et al* 2008 Artificial dirt: microfluidic substrates for nematode neurobiology and behavior *J. Neurophysiol.* **99** 3136–43
- [17] Park S *et al* 2008 Enhanced *Caenorhabditis elegans* locomotion in a structured microfluidic environment *PLoS One* **3** e2550
- [18] Niebur E and Erdös P 1991 Theory of the locomotion of nematodes: dynamics of undulatory progression on a surface *Biophys. J.* **60** 1132–46
- [19] Wakabayashi M. 2006 Computational plausibility of stretch receptors as the basis for motor control *C. elegans* BA Thesis School of Information Technology & Electrical Engineering, Univ. of Queensland, Australia
- [20] Madden J D W *et al* 2004 Artificial muscle technology: physical principles and naval prospects *IEEE J. Ocean. Eng.* **29** 706–28
- [21] Nagahico S and Geoffrey S 2004 Use of a shape memory alloy for the design of an oscillatory propulsion system *IEEE J. Ocean. Eng.* **29** 750–5
- [22] Nakabo Y, Mukai T and Asaka K 2007 Biomimetic soft robots using IPMC *Electroactive Polymers for Robotic Applications* (Berlin: Springer)
- [23] Carpi F and Rossi D D 2006 Biomimetic dielectric elastomer actuators *Proc. IEEE/RAS-EMBS Int. Conf. BioRob* pp 1073–8
- [24] Zhang Q and Scheinbeim J 2001 Electric EAP *Electroactive Polymer Actuators as Artificial Muscle* ed Y Bar-Cohen (Bellingham, WA: SPIE Press)
- [25] Suzuki M, Goto T, Tsuji T and Ohtake H 2005 A dynamic body model of the nematode *C. elegans* with neural oscillators *J. Robot. Mechatronics* **17** 318–26
- [26] Ma N and Song G 2003 Control of shape memory alloy actuator using pulse width modulation *Smart Mater. Struct.* **12** 712–9
- [27] Kim D, Park S, Mahadevan L and Shin J H 2011 The shallow turn of a worm *J. Exp. Biol.* **214** 1554–9